EEG amplitude modulation analysis for semi-automated diagnosis of Alzheimer's disease

EURASIP JOURNAL ON ADVANCES IN SIGNAL PROCESSING, CHAM, v. 18, n. 52, supl. 1, Part 2, pp. 16890-16901, DEC, 2012
http://www.producao.usp.br/handle/BDPI/37872

EURASIP Journal on Advances in Signal Processing
a SpringerOpen Journal

RESEARCH Open Access

EEG amplitude modulation analysis for semi-automated diagnosis of Alzheimer's disease

Tiago H Falk[1*], Francisco J Fraga[2], Lucas Trambaiolli[3] and Renato Anghinah[4]

Abstract

Recent experimental evidence has suggested a neuromodulatory deficit in Alzheimer's disease (AD). In this paper, we present a new electroencephalogram (EEG) based metric to quantitatively characterize neuromodulatory activity. More specifically, the short-term EEG amplitude modulation rate-of-change (i.e., modulation frequency) is computed for five EEG subband signals. To test the performance of the proposed metric, a classification task was performed on a database of 32 participants partitioned into three groups of approximately equal size: healthy controls, patients diagnosed with mild AD, and those with moderate-to-severe AD. To gauge the benefits of the proposed metric, performance results were compared with those obtained using EEG spectral peak parameters which were recently shown to outperform other conventional EEG measures. Using a simple feature selection algorithm based on area-under-the-curve maximization and a support vector machine classifier, the proposed parameters resulted in accuracy gains, relative to spectral peak parameters, of 21.3% when discriminating between the three groups and by 50% when mild and moderate-to-severe groups were merged into one. The preliminary findings reported herein provide promising insights that automated tools may be developed to assist physicians in very early diagnosis of AD as well as provide researchers with a tool to automatically characterize cross-frequency interactions and their changes with disease.

Keywords: Alzheimer's disease, Modulation spectrum, Electroencephalogram, Spectral peak, Support vector machine

Introduction

Alzheimer's disease (AD) is considered to be the main cause of dementia in Western countries [1]. A recent study suggests that 60–80% of dementia cases in the United States are due to AD [2], amounting to $172 billion in health care costs; worldwide, this number rises to $604 billion [3]. Alzheimer's disease is commonly manifested by loss of memory and other intellectual abilities which often result in interference of daily life. Currently, diagnosis of AD is done via neuropsychological evaluations, with accuracies ranging from 85–93% in university hospitals. These evaluations require experienced professionals as well as lengthy sessions. Notwithstanding, definitive diagnosis can only be established with a histo-pathological analysis of the brain (i.e., autopsy or biopsy) [4]. Hence, the search for an accurate biological marker for early diagnosis of the disease remains an open challenge.

In the last two decades, there has been a push to develop objective tools capable of assisting physicians in the early diagnosis of the disease. Since AD is a cortical dementia, the quantitative electroencephalogram (qEEG) has merged as a prominent candidate (henceforth, the terminology 'EEG' will be used for simplicity). The EEG signal reflects functional changes in the cerebral cortex of the patient. For the purpose of AD diagnosis, two branches of EEG signal analysis have emerged: spectral and nonlinear dynamics [5]. Pioneering spectral analysis studies showed that AD patients presented increased activity in the delta (0.1–4 Hz) and theta (4–8 Hz) frequency bands, as well as decreased activity in the alpha (8–12 Hz) and beta (12–30 Hz) bands [6-11], thus suggesting a slowing of the EEG signal. Moreover, reduced spectral coherence between the two hemispheres was shown between the alpha and beta frequency bands [12-16]. These spectral

*Correspondence: falk@emt.inrs.ca
[1] Institut National de la Recherche Scientifique, Energy, Materials, and Telecommunications, University of Quebec, Montréal, Quebec, Canada
Full list of author information is available at the end of the article

differences were also shown to be correlated with disease progression [13,17-19].

Nonlinear dynamics analysis, in turn, aims at measuring the cortical complexity of the brain by quantifying the complexity or "chaos" in EEG temporal patterns. Mathematical complexity measures such as the Lyapunov exponent, surrogate data analysis, entropy, or even artificial neural networks have been proposed in the past. In general, studies have agreed that AD causes a decrease in EEG pattern complexity [20-26], a factor likely caused by the reduction in non-linear connections between cortical regions, neuronal death, or even deficiency of neurotransmitters [27]. One major limiting factor in the widespread use of nonlinear dynamic models in AD classification is the high sensitivity of available methods to algorithm parameter changes. As such, a large pool of patient data is needed in order to obtain the optimal algorithm parameter values needed for reliable and repeatable analysis. Recent studies have suggested, nonetheless, that the two phenomena described above are strongly related, i.e., a strong correlation exists between EEG slowing and loss of complexity [28].

In this article, we propose an alternate nonstationary EEG analysis method for (semi-)automated AD diagnosis, based on extending earlier study reported in [29]. More specifically, we measure the rate at which subband EEG amplitude modulations change over short periods of time (circa 5 s) and compare such "spectro-temporal" signal representations between healthy controls and patients with varying AD severity levels (ranging from mild to severe). The study was motivated by recent findings in the AD treatment literature which suggested that neuromodulatory deficits seen with AD could be treated via deep brain stimulation [30]. According to the hemoneural hypothesis, cerebral hemodynamics play an important role in information processing via the modulation of neural activity [31]. Since impaired cerebral blood flow is a hallmark in AD (e.g., [32,33]), quantitative measurement of neuromodulatory activity may provide a useful tool for automated characterization of Alzheimer's disease. In addition, the proposed spectro-temporal analysis technique allows for direct characterization of cross-frequency interaction effects (by measuring rates at which EEG subbands are modulated), thus provides complementary information to conventional frequency and time-frequency methods. For example, relative to conventional spectral power analyzes which have shown overall EEG "slowing," [28], the proposed measure allows for insights into which "waves" (i.e., modulation frequencies) ride each EEG subband signal and their interactions over time.

The remainder of this article is organized as follows. Section 'Materials and methods' describes the materials and methods used in the experiment, including the proposed and benchmark parameters. This is followed by Sections 'Experimental results', 'Discussion', and 'Conclusion', respectively.

Materials and methods

Participants

Data used in this study were extracted from a clinical database comprised of resting-awake multi-channel EEG recordings from 32 individuals, separated into three groups of roughly the same size. Alzheimer's disease diagnosis was made by experienced physicians at the Reference Center of Behavioral Disturbances and Dementia, School of Medicine, at the Universidade de São Paulo (Brazil) according to the well-established NINCDS-ADRDA criteria [34] and classified according to the mini-mental state examination (MMSE) and the the clinical dementia rating (CDR) scale. Table 1 shows the demographics of the participants. All three groups are education-matched and groups 'control' and 'moderate-to-severe' are also age-matched (according to a statistical t-test with 5% significance level). Participants had no history of diabetes mellitus, kidney diseases, thyroid diseases, alcoholism, liver disease, lung disease, or vitamin B12 deficiency, factors which could also lead to cognitive impairment. Ethics approval was obtained from the affiliated institutes and participants provided written consent.

Data collection and pre-processing

Multi-channel EEG (19 channels) signals were collected using the *Braintech 3.0* instrumentation (EMSA Equipamentos Médicos Inc., Brazil), digitized with a 12-bit analog-to-digital converter and sampled at a rate of 200 Hz; impedance was maintained below 10 kΩ. Placement of scalp electrodes (referential montage) followed the international 10–20 system. Biauricular referential electrodes were attached, as recommended by the Brazilian Society of Clinical Neurophysiology and the

Table 1 Participant demographics: last three columns represent average ± standard deviation and columns labeled 'Age' and 'Education' are given in years

Group	Total	Female	Age	Education	MMSE
Controls	11	6	68.1 ± 7.1	7.9 ± 5.1	26.6 ± 2.7
Mild AD	11	8	75.9 ± 4.1	4.2 ± 3.5	18.5 ± 4.7
Moderate-to-severe AD	10	9	68.4 ± 8.8	5.0 ± 4.0	14.8 ± 3.9

American EEG Society. Motivated by our recent findings [35,36], from the referential montage we derived a virtual interhemispheric bipolar montage, as there is evidence of an interhemispheric disconnection in AD [27]. The so-called "bipolar signal" was obtained by simply subtracting the two bi-auricular referenced signals involved [37]. In our experiments, the electrode pairs included: F3–F4, F7–F8, C3–C4, T3–T4, P3–P4, T5–T6, and O1–O2. During examination, EEG was recorded with the participants awake and resting with their eyes closed. An infinite impulse response low-pass elliptic filter with a zero at 60 Hz was applied to eliminate any power grid interference. For each participant, 48 s epochs were selected per EEG channel by an experienced physician. The selected epochs were free of eye movement, electromyographic activity, and head motion artifacts. Given this human intervention requirement, the proposed system is deemed "semi-automated;" nonetheless, a fully automated system may be possible with the use of intelligent artifact removal techniques such as independent component analysis (see Section 'Discussion').

Spectro-temporal EEG amplitude modulation analysis

Spectro-temporal signal analysis has been shown useful in other physiological domains, such as heart and lung sound separation [38], pulmonary adventitious sound analysis [39], dysphonia recognition [40], and speech acoustics analysis [41]. As argued by [42], "the presence of amplitude modulation in bioelectrical processes is of fundamental nature, since it is a direct reflection of the control, synchronization, regulation, and intersystem interaction in the nervous and other body systems." With AD, a neuromodulatory deficit may exist due to impaired cerebral blood flow [31], particularly involving the so-called resting state networks [43]. By quantitatively characterizing resting-awake EEG amplitude modulation differences between healthy and AD patients, automated disease characterization may be made possible, thus assisting clinicians with diagnostics. This study describes the first steps towards the development of one such (semi-)automated diagnostic tool.

Figure 1 depicts the signal processing steps involved in the calculation of spectro-temporal EEG amplitude modulation representation. First, the fullband resting-awake EEG signal $s(n)$ is decomposed into five subband signals $s_i(n) = s(n) * h_i(n)$, where $h_i(n)$, $i = 1, \ldots, 5$ are the impulse responses of elliptic bandpass filters used to separate delta (0.1–4 Hz), theta (4–8 Hz), alpha (8–12 Hz), beta (12–30 Hz), and gamma (30–100 Hz) bands [44]. The temporal amplitude envelope of each of the five subband EEG signals is then computed by means of a Hilbert transform $\mathcal{H}\{\cdot\}$ (the interested reader is referred to [45] and references therein for more details). The temporal envelopes $e_i(n)$, or amplitude modulations, are computed as the magnitude of the complex analytic signal $\tilde{s}_i(n) = s_i(n) + j\mathcal{H}\{s_i(n)\}$, i.e.,

$$e_i(n) = \sqrt{s_i(n)^2 + \mathcal{H}\{s_i(n)\}^2}. \tag{1}$$

The subplots on the right of Figure 1 illustrate representative EEG subband signals (gray) and their respective Hilbert amplitude envelopes (black).

Temporal envelopes are then multiplied by a 5 s Hamming window with 500 ms shifts; the windowed envelope for frame m is represented as $e_i(m, n)$, where n is the time variable. Frames of 5 s duration are used in order to obtain accurate resolution in the new so-called modulation frequency domain and to keep consistency with the benchmark parameter described in Section 'Benchmark parameters'. The so-called "modulation spectral" representation for EEG subband i is obtained by taking the discrete Fourier transform $\mathcal{F}\{\cdot\}$ of the temporal envelope $e_i(m, n)$, i.e.,

$$E_i(m; f) = |\mathcal{F}\{e_i(m, n)\}|, \tag{2}$$

where f denotes modulation frequency. In order to directly quantify the rate of change of the subband temporal envelopes and possible cross-frequency interactions, modulation frequency bins are further grouped into four bands empirically designed to coincide with the range of the first four conventional frequency bands (i.e., delta-beta). This choice was driven by the fact that, by definition of the Hilbert transform, the envelope signal can only contain frequencies (i.e., modulation frequencies) up to the maximum frequency of its originating signal (i.e., following the so-called Bedrosian's theorem [46,47]). As such, gamma-level modulation frequencies would only be present in the gamma frequency band. Hence, to reduce data dimensionality, the so-called gamma modulation band is not considered here.

Henceforth, to distinguish between modulation and frequency bands, we will refer to the former as m-delta (0.1–4 Hz), m-theta (4–8 Hz), m-alpha (8–12 Hz), and m-beta (12–30 Hz). The notation $\mathcal{E}_{i,j}(m)$ and $\overline{\mathcal{E}}_{i,j}$ will be used to denote the per-frame and average (over all frames in an EEG epoch) modulation energy of the ith subband signal grouped by the jth modulation filter. The latter can be viewed as an average modulation spectrogram which conveys information as to how fast (horizontal axis) each of the five subband envelopes (vertical axis) are modulated over short periods of time (i.e., 5 s in our analyzes). The bottom left and right plots of Figure 1, for example,

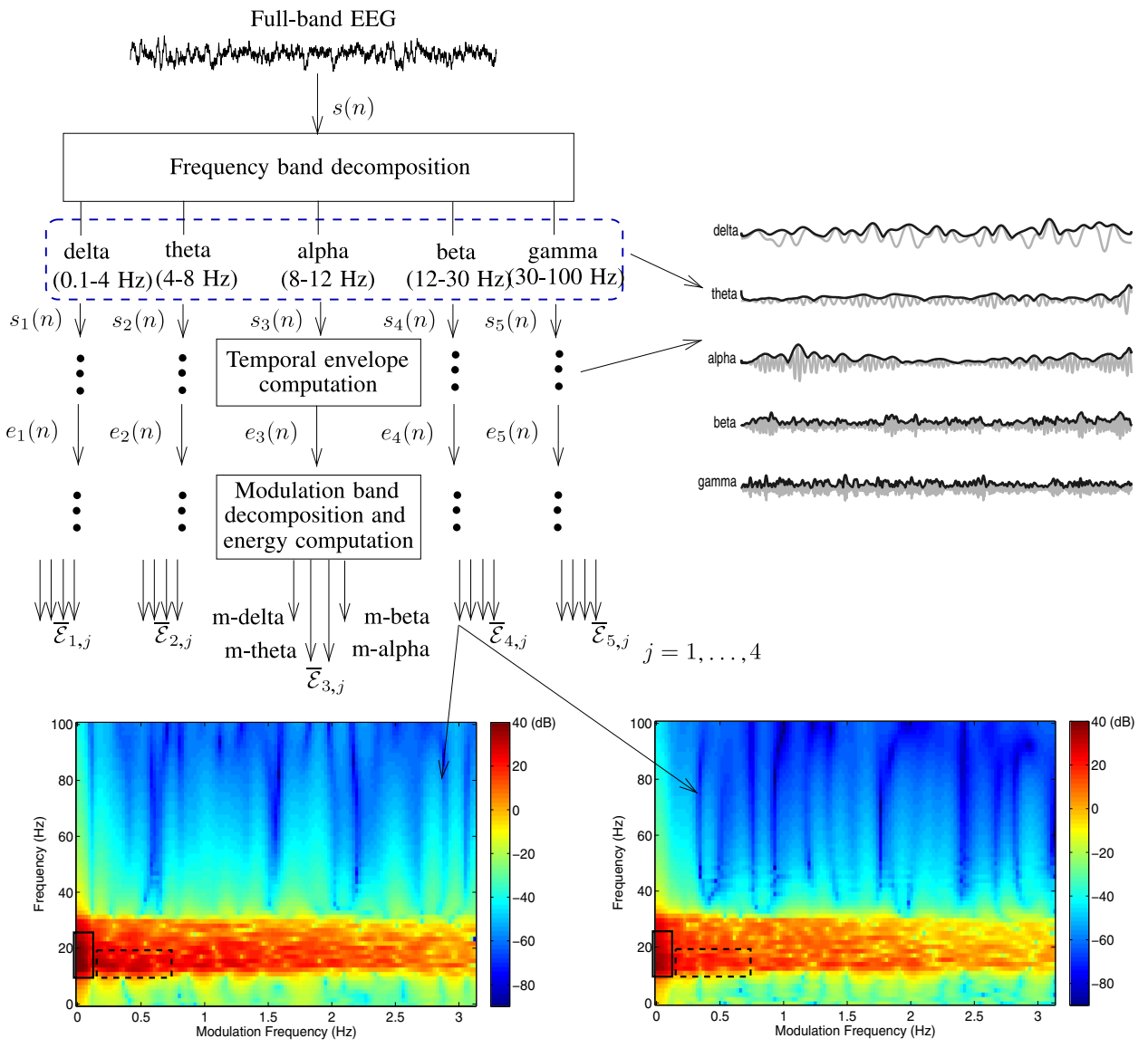

Figure 1 Signal processing steps used to compute the EEG spectro-temporal signal representation. Subplots on the top right illustrate the five subband EEG signals (gray) and their respective Hilbert temporal envelopes (black). The subplots on the bottom depict the average modulation spectrograms for the beta frequency and m-delta modulation bands (i.e., $\overline{\boldsymbol{\mathcal{E}}}_{4,1}$, where only a part of the *m*-delta band is depicted for visualization purposes) for healthy control (left subplot) and AD (right subplot) patients.

depict $\overline{\mathcal{E}}_{4,1}$ (i.e., beta frequency, *m*-delta modulation frequency) for healthy control and moderate AD patients, respectively. From the plots it can be seen that decreased activity in the beta frequency band is observed with AD (see solid-line rectangle centered at ∼0 Hz modulation frequency), thus corroborating previous findings [27]. The modulation spectrum, however, provides an additional dimension to extract information from. For example, in the dashed rectangle centered at ∼0.5 Hz modulation frequency, it can be seen that with AD, decreased modulation frequency content is also observed. Modulation energy "ratio" parameters are computed by means of a new proposed parameter termed *percentage modulation energy* (PME), which is given by:

$$\mathrm{PME}_{i,j} = \frac{\overline{\mathcal{E}}_{i,j}}{\sum_{i=1}^{5}\sum_{j=1}^{4}\overline{\mathcal{E}}_{i,j}} \times 100\%, \tag{3}$$

for each of the 7 bipolar signals. In total, 140 (20 PMEs × 7 bipolar signals) features are extracted. As mentioned above, however, due to Bedrosian's theorem, only 98 of these features (14 PMEs × 7 bipolar signals) convey useful information, thus are used throughout the remainder

of this article. In our experiments, feature selection is used in order to sift only salient features for the classification task at hand. Feature selection and classifier design are described in Section 'Salient feature selection and classifier design.'

Benchmark parameters

In order to gauge the benefits of the proposed PME parameters, a classifier trained on EEG 'spectral peak' parameters was used as benchmark. Spectral peak, as the name suggests, corresponds to the frequency at which the magnitude of the EEG spectrum reaches its maximum value. Its computation involves the use of a fast fourier transform (FFT) of windowed EEG segments. Since the EEG signals used in this study were recorded with subjects resting and with eyes closed, they reflect only the spontaneous brain activity, which is in most part nonstationary [44]. Consequently, this demands the need to use sliding windows in order to deal with the nonstationarity. Each epoch comprises 8 s and we used 5 s Hamming windows with 90% overlap, thus leading to seven frames for each epoch. Previous studies have suggested that classifiers trained on the spectral peak parameter outperform those trained with more conventional parameters, such as spectral coherence [48]. As with the PME features, five frequency bands were used (delta, theta, alpha, beta, and gamma) and spectral peak parameters were computed for each band. Additionally, our previous experiments have suggested that spectral peak parameters computed from a bipolar electrode montage are more reliable than those computed from a referential montage [35]. As a consequence, the same inter-hemispheric bipolar montage used to compute the PME features was used (i.e., electrode pairs F3–F4, F7–F8, C3–C4, T3–T4, P3–P4, T5–T6, and O1–O2) totaling 35 possible spectral peak features (5 bands $\times$ 7 bipolar signals).

Salient feature selection and classifier design

In order to reduce the high-dimensional PME feature space into one that is feasible for classifier design, a feature selection algorithm based on maximization of the area under the curve (AUC) was used; the reader is referred to [49] for more details. In our experiments, 10 EEG epochs (out of a total of 40 epochs) per participant were randomly selected and set aside for feature selection. The remaining 30 epochs were used for classifier training/testing using a leave-one-out cross-validation paradigm. A total of 35 salient PME features were selected in order for fair comparisons to be made with the benchmark parameters (see Section 'Benchmark parameters'); such dimensionality is inline with those reported in the literature (e.g., [50]). Table 2 shows the top-35 salient PME features and their ranks. In the table, features are represented using a "Bipol-Band-ModBand" notation where 'Bipol' indicates the bipolar signal (e.g., T5–T6), 'Band' indicates the frequency band, and 'ModBand' the modulation band.

Once salient features were selected, a support vector machine classifier (SVC) was designed. SVCs provide numerous computational and algorithmic advantages over artificial neural networks, as highlighted in [51], and have been shown useful for automated AD diagnosis based on spectral peak [48] and other conventional parameters [50]. A complete description of SVM classification is beyond the scope of this article and only a brief summary is presented here; the interested reader is referred to [52,53] and the references therein for more detail. The basic principle behind SVM classification is to map features into a higher dimension by means of a kernel function. In the higher-dimensional space, features between different classes become linearly separable and (maximum-margin) hyperplanes can be obtained [52,53]. SVM classification is a supervised learning method, thus labeled data are needed. Commonly,

Table 2 Top-35 salient PME features selected via an AUC-maximization based feature selection algorithm

Feature	Rank	Feature	Rank	Feature	Rank
F7-F8—theta—m-delta	1	F3-F4—theta—m-delta	13	T3-T4—beta—m-theta	25
O1-O2—beta—m-alpha	2	C3-C4—theta—m-theta	14	F7-F8—beta—m-alpha	26
T5-T6—beta—m-theta	3	O1-O2—beta—m-delta	15	C3-C4—beta—m-delta	27
P3-P4—beta—m-delta	4	F3-F4—theta—m-theta	16	F7-F8—beta—m-delta	28
F7-F8—theta—m-theta	5	P3-P4—beta—m-theta	17	T3-T4—beta—m-delta	29
C3-C4—beta—m-theta	6	T5-T6—beta—m-alpha	18	O1-O2—theta—m-theta	30
O1-O2—theta—m-delta	7	C3-C4—beta—m-alpha	19	F3-F4—gamma—m-beta	31
T5-T6—theta—m-theta	8	C3-C4—theta—m-delta	20	F7-F8—alpha—m-delta	32
P3-P4—beta—m-alpha	9	C3-C4—beta—m-beta	21	P3-P4—theta—m-theta	33
T5-T6—beta—m-delta	10	T3-T4—theta—m-theta	22	T3-T4—beta—m-alpha	34
T5-T6—theta—m-delta	11	F7-F8—beta—m-theta	23	T5-T6—delta—m-delta	35
T3-T4—theta—m-delta	12	O1-O2—beta—m-theta	24		

a radial basis function (RBF) is used as the kernel. In our experiments, the Weka RBF-SVC implementation was used [54] with the following default parameter values: regularization coefficient $C = 1$ and $\gamma = 0.01$). A leave-one(epoch)-out (LOO) cross-validation paradigm was used for classifier design and testing.

Experimental results

Based on the LOO paradigm, different performance metrics are used. First, classifier accuracy is reported for the three-class discrimination task (i.e., control vs. mild vs. moderate/severe). Second, classifier overall accuracy, sensitivity, and specificity are reported for a two-class 'control vs. AD' discrimination task where mild and moderate-to-severe patients are pooled into one group. Classifier sensitivity measures the percentage of correctly classified epochs belonging to AD patients, whereas specificity measures the percentage of correctly classified epochs belonging to healthy controls; all metrics are expressed in percentage values. For the three-class task, overall accuracies of 65.6 and 56.3% were obtained with PME and spectral peak parameters, respectively, thus were significantly greater than chance ($p < 10^{-5}$ and $p < 0.003$, respectively, using a t-test). In order to quantify improvements obtained by using the proposed parameters, a relative "accuracy-gain" metric is used, thus characterizing the relative improvement to perfect classification. The metric is given by:

$$\text{Acc-Gain} = \frac{\text{Acc}_{\text{PME}} - \text{Acc}_{\text{peak}}}{100 - \text{Acc}_{\text{peak}}} \times 100\%, \tag{4}$$

where 'Acc_{PME}' and 'Acc_{peak}' denote the accuracy (or sensitivity/specificity) obtained with the proposed and benchmark parameters, respectively. As such, a 21.3% relative accuracy gain is obtained. Additionally, Table 3 reports the overall classifier accuracy, sensitivity and specificity for the proposed PME features along with the benchmark spectral peak parameters for the two-class task. As can be seen, specificity gains of up to 67% can be attained with the proposed parameters.

Table 3 Performance comparison between proposed and benchmark parameters

Metric	PME (%)	Spectral peak (%)	Acc-Gain (%)
Accuracy	90.6	81.3	49.7
Sensitivity	90.5	85.7	33.6
Specificity	90.9	72.7	66.7

Column labeled 'Acc-Gain' represents the percentage "accuracy-gain" obtained with proposed PME parameters, as per Equation (4).

Discussion

Feature ranking

As observed from Table 2, features extracted from the frontal, occipital, temporal, and parietal regions constitute the five highest ranking features with two of them representing long-distance connections (F7–F8). Interestingly, these are areas that are critically affected by Alzheimer's disease [55] and that have also been shown to be prone to impaired cerebral blood flow [56]. Future studies should focus on multimodal neuroimaging techniques to further explore the possibility of a neurovascular coupling deficit with AD. Moreover, it was observed that salient PME features were extracted almost exclusively from theta and beta frequency bands with delta and alpha band features being completely discarded. Previous studies based on spectral coherence parameters, on the other hand, have reported significant differences between AD and healthy control groups in the alpha band over several regions of the brain (e.g., [57]). EEG complexity/chaoticity experiments have also uncovered significant differences between the two groups in the alpha band, particularly in the right frontal and left parieto-occipital regions [58], as well as in the beta band across multiple brain regions [59]. The findings reported here suggest that the proposed PME parameters may be complementary to such conventional EEG parameters, thus further improvements in classification accuracy may be possible by combining multiple parameters. Our experiments with combined PME and spectral peak parameters, however, did not suggest complementarity between these two modalities. Lastly, it was observed that the majority of the selected features corresponded to m-delta and m-theta modulation frequencies, suggesting that the most significant impairments occur in slowly-varying amplitude modulations.

Semi-automated disease characterization

In regards to classification, the proposed PME features were shown to outperform the benchmark parameters both on the two- and three-class discrimination tasks. As part of an exploratory analysis, three other two-class tasks were performed, namely: controls vs. mild; controls vs. moderate/severe; and mild vs. moderate/severe. It was observed that for all three experiments above, the accuracies of the classifiers trained using spectral peak parameters were: 54.5% ($p > 0.26$), 66.7% ($p < 0.04$), and 47.6% ($p > 0.5$), respectively, thus only 'controls vs. moderate/severe' accuracy was significantly different from chance (binomial test). On the other hand, for the PME parameters, the accuracies were: 74.1% ($p < 0.008$), 71.4% ($p < 0.014$), and 53.8% ($p > 0.33$), respectively, thus the 'controls vs. mild' and 'controls vs. moderate/severe' classification accuracies were significantly greater than chance (binomial test). These results suggest that the proposed PME parameters are promising features for semi-

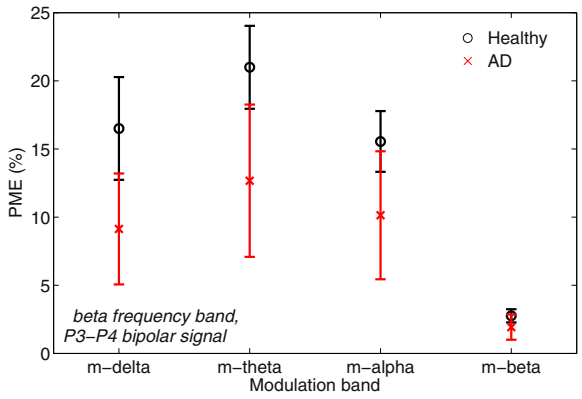

Figure 2 Proposed beta-band PME parameter averaged over all AD and healthy controls Plots are for the P3–P4 bipolar signal.

automated (early) diagnosis of AD. Regarding the latter scenario (mild versus moderate/severe), it is conjectured that the observed drop in performance was due to the sensitiveness of the PME parameters to the wide range of disease severity levels ($2 \leq \text{CDR} \leq 3$) pooled into the moderate/severe group. Given the size limitations of the available dataset, it was not possible for the moderate/severe class to be separated into two, such that this hypothesis could be tested; this is left for future investigation.

Cross-frequency interaction

As mentioned previously, the proposed spectro-temporal analysis technique allows for direct characterization of EEG cross-frequency interaction effects and their changes with AD. Beta-theta interaction, for example, has been previously linked to working memory performance [60] and reward-gain motivation [61] in healthy adults. Interestingly, in our experiments it was observed that $\text{PME}_{4,2}$ (i.e., beta rhythms modulated at a theta rate) was more pronounced in healthy controls than in AD patients, as depicted by Figure 2. Such findings suggest that resting-awake EEG theta-beta interaction is impaired with AD. While the plot is representative of the parietal region (P3-P4), similar behavior was observed across the midline, central, temporal, and frontal regions. It is hypothesized that the reduced cross-frequency interaction observed in the AD population may be related to certain behavioral and psychological symptoms observed with the disease, such as lack of interest [62]. Ultimately, it is hoped that the proposed parameters will allow for other cross-frequency interactions to be explored, such as theta-gamma which was recently linked to memory impairment [63].

Study limitations

Findings reported here are based on a limited sample size of 32 participants, 21 of which have been diagnosed with AD of varying severity levels ranging from mild to severe. This limited number of participants may cause issues with classifier over-training, which would lead to poor generalization ability on "unseen" patients. In order to investigate if the developed classifiers were overfit to the available data, an additional leave-one-patient-out cross-validation test was performed where data from 31 patients were used during training and data from the remaining patient was used for testing. Accuracy, sensitivity and specificity of approximately 91% were obtained, thus inline with those reported in Table 3. These findings suggest that the developed classifiers were not overfit and provide good generalization ability. Future studies, nonetheless, should focus on a larger, more gender-balanced participant pool, as gender differences may also play a factor, as reported by [64]. Moreover, our findings have been based on artefact-free EEG epochs manually selected by an experienced neurophysiologist. In order to develop a fully automated diagnostic tool, automated artifact removal techniques, such as independent component analysis [65], need to be explored and their effects on the PME parameters need to be quantified. This is the focus of our ongoing investigations.

Conclusion

This article proposed an innovative spectro-temporal EEG signal representation with which salient features were extracted for semi-automated characterization of Alzheimer's disease (AD). When tested on a limited dataset of 32 participants (11 controls, 11 mild AD, and 10 moderate-to-severe AD), experimental results showed that classifiers trained on the proposed features outperformed those trained on benchmark spectral peak parameters. The proposed parameters also seem to be useful for EEG cross-frequency interaction investigations and suggested that theta-beta interaction may be reduced with AD.

Competing interests
The authors declare that they have no competing interest.

Author details
[1]Institut National de la Recherche Scientifique, Energy, Materials, and Telecommunications, University of Quebec, Montréal, Quebec, Canada. [2]Engineering, Modeling and Applied Social Sciences Center, Universidade Federal do ABC, Santo André, Brazil. [3]Mathematics, Computing and Cognition Center, Universidade Federal do ABC, Santo André, Brazil. [4]Reference Center of Behavioral Disturbances and Dementia, School of Medicine, Universidade de São Paulo, São Paulo, Brazil.

Received: 6 December 2011 Accepted: 23 July 2012
Published: 30 August 2012

References

1. T Bird, in *Harrison's principles of internal medicine, E Braunwald et al. (eds.)* Alzheimer's disease and other primary dementias. (McGraw-Hill, New York, 2001), pp. 2391–2399
2. Alzheimer Association, Alzheimer's disease facts and figures: 2010 report. Alzheimers Dement. **6**(2), 158–194 (2010)

3. World Alzheimer report 2010: The global economic impact of dementia, Alzheimer Disease International, Tech. Rep. pp. 56 (2010)
4. D Terry, Neuropathological changes in Alzheimer disease. Prog. Brain Res. **101**, 383–390 (1994)
5. J Dauwels, F Vialatte, A Cichocki, Diagnosis of Alzheimer disease from EEG signals: Where are we standing? Current Alzheimer Res. **7**(6), 487–505 (2010)
6. R Brenner, R Ulrich, D Spiker, R Sclabassi, C Reynolds, R Marin, F Boller, Computerized EEG spectral analysis in elderly normal, demented and depressed subjects. Electroenceph. Clin. Neurophysiol. **64**, 483–492 (1986)
7. L Coben, W Danziger, L Berg, Frequency analysis of the resting awake EEG in mild senile dementia of Alzheimer type. Electroenceph. Clin. Neurophysiol. **55**(4), 372–380 (1983)
8. L Coben, W Danziger, M Storandt, A longitudinal EEG study of mild senile dementia of Alzheimer type: changes at 1 year and at 2.5 years. Electroenceph. Clin. Neurophysiol. **61**(2), 101–112 (1985)
9. A Arenas, R Brenner, C Reynolds, Temporal slowing in the elderly revisited. Am. J. EEG Technol. **26**, 105–114 (1986)
10. S Giaquinto, G Nolfe, The EEG in the normal elderly: a contribution to the interpretation of aging and dementia. Electroenceph. Clin. Neurophysiol. **63**(6), 540–546 (1986)
11. D Cibils, Dementia and qEEG (Alzheimer's disease). Clin. Neurophysiol. **54**, 289–294 (2002)
12. C Besthorn, H Forstl, C Geiger-Kabisch, H Sattel, T Gasser, U Schreiter-Gasser, EEG coherence in Alzheimer disease. Electroenceph. Clin. Neurophysiol. **90**(3), 242–245 (1994)
13. J Dunkin, A Leuchter, T Newton, I Cook, Reduced EEG coherence in dementia: state or trait marker? Biol. Psychiat. **35**(11), 870–879 (1994)
14. A Leuchter, J Spar, D Walter, H Weiner, Electroencephalographic spectra and coherence in the diagnosis of Alzheimer's-type and multi-infarct dementia: a pilot study. Arch. Gen. Psychiat. **44**(11), 993 (1987)
15. T Locatelli, M Cursi, D Liberati, M Franceschi, G Comi, EEG coherence in Alzheimer's disease. Electroenceph. Clin. Neurophysiol. **106**(3), 229–237 (1998)
16. E Sloan, G Fenton, N Kennedy, J MacLennan, Neurophysiology and SPECT cerebral blood flow patterns in dementia. Electroenceph. Clin. Neurophysiol. **91**(3), 163–170 (1994)
17. J Hughes, S Shanmugham, L Wetzel, S Bellur, C Hughes, The relationship between EEG changes and cognitive functions in dementia: a study in a VA population. Clin. Electroencephal. **20**(2), 77–85 (1989)
18. V Jelic, Early diagnosis of, AD, Ph.D. dissertation, (Karolinska Institutet, Stockholm, 1996)
19. J Kowalski, M Gawel, A Pfeffer, M Barcikowska, The diagnostic value of EEG in Alzheimer disease: correlation with the severity of mental impairment. J. Clin. Neurophysiol. **18**(6), 570–575 (2001)
20. B Jelles, J Van Birgelen, J Slaets, R Hekster, E Jonkman, C Stam, Decrease of non-linear structure in the EEG of Alzheimer patients compared to healthy controls. Clin. Neurophysiol. **110**(7), 1159–1167 (1999)
21. J Jeong, J Gore, B Peterson, Mutual information analysis of the EEG in patients with Alzheimer's disease. Clin. Neurophysiol. **112**(5), 827–835 (2001)
22. A Villa, I Tetko, P Dutoit, G Vantini, Non-linear cortico-cortical interactions modulated by cholinergic afferences from the rat basal forebrain. Biosystems. **58**, 219–228 (2000)
23. D Abasolo, R Hornero, P Espino, J Poza, C Sanchez, R dela Rosa, Analysis of regularity in the EEG background activity of Alzheimer's disease patients with approximate entropy. Clin. Neurophysiol. **116**(8), 1826–1834 (2005)
24. D Abasolo, R Hornero, C Gomez, M Garcia, M Lopez, Analysis of EEG background activity in Alzheimer's disease patients with Lempel-Ziv complexity and central tendency measure. Med. Eng. Phys. **28**(4), 315–322 (2006)
25. M Buscema, P Rossini, C Babiloni, E Grossi, The IFAST model, a novel parallel nonlinear EEG analysis technique, distinguishes mild cognitive impairment and Alzheimer's disease patients with high degree of accuracy. Artif. Intell. Med. **40**(2), 127–141 (2007)
26. P Rossini, M Buscema, M Capriotti, E Grossi, G Rodriguez, C Del Percio, C Babiloni, Is it possible to automatically distinguish resting EEG data of normal elderly vs. mild cognitive impairment subjects with high degree of accuracy? Clin. Neurophysiol. **119**(7), 1534–1545 (2008)
27. J Jeong, EEG dynamics in patients with Alzheimer's disease. Clin. Neurophysiol. **115**(7), 1490–1505 (2004)
28. D Justin, K Srinivasan, M Ramasubba Reddy, M Toshimitsu, V François-Benoît, L Charles, J Jaeseung, C Andrzej, Slowing and loss of complexity in Alzheimer's EEG: Two sides of the same coin? Int J Alzheimer's Disease. **2011**(Article ID 539621), 10 (2011). doi:10.4061/2011/539621
29. L Trambaiolli, TH Falk, F Fraga, R Anghinah, A Lorena, in *Proc IEEE-EMBC,* vol. 1 EEG spectro-temporal modulation energy: a new feature for automated diagnosis of Alzheimer's disease. (Boston, USA, 2011), pp. 3828-3831
30. A Laxton, D Tang-Wai, M McAndrews, D Zumsteg, R Wennberg, R Keren, J Wherrett, G Naglie, C Hamani, G Smith, A Lozano, A phase I trial of deep brain stimulation of memory circuits in Alzheimer's disease. Ann. Neurol. **8**(4), 521–534 (2010)
31. C Moore, R Cao, The hemo-neural hypothesis: on the role of blood flow in information processing. J. Neurophysiol. **99**, 2035–2047 (2008)
32. A van Beek, J Lagro, M Olde-Rikkert, R Zhang, J Claassen, Oscillations in cerebral blood flow and cortical oxygenation in Alzheimer's disease. Neurobiol. Ag. **33**(2), 428.e21-428.31 (2011). doi:10.1016/j.neurobiolaging.2010.11.016
33. J Zeller, M Herrmann, A Ehlis, T Polak, A Fallgatter, Altered parietal brain oxygenation in Alzheimer's disease as assessed with near-infrared spectroscopy. Am. J. Geriatr. Psychiatry. **18**(5), 433–441 (2010)
34. G McKhann, D Drachman, M Folstein, R Katzman, D Price, E Stadlan, Clinical diagnosis of Alzheimer's disease: report of the NINCDS-ADRDA work group. Neurology. **34**(7), 939 (1984)
35. L Trambaiolli, A Lorena, F Fraga, P Kanda, R Anghinah, R Nitrini, Improving Alzheimer's disease diagnosis with machine learning techniques. Clinic. EEG Neurosci. **42**(3), 160–165 (2011)
36. L Trambaiolli, T Falk, F Fraga, A Lorena, R Anghinah, in *Proc. Intl. Conf. IEEE EMBS,* vol. 1 EEG spectro-temporal modulation energy: a new feature for automated diagnosis of Alzheimer's disease. (Boston, USA, 2011), pp. 3828–3831
37. P Nunez, R Srinivasan, *Electric fields of the brain: the neurophysics of EEG* (Oxford University Press, USA, 2006)
38. T Falk, W Chan, in *Proc Int. Conf. IEEE-EMBS,* vol. 1 Modulation filtering for heart and lung sound separation from breath sound recordings. (Vancouver, Canada, 2008), pp. 1859–1862
39. TH Falk, W-Y Chan, E Sejdic, T Chau, *New Developments in Biomedical Engineering* InTech, 2010, ch. Spectro-temporal Anlysis of Auscultatory Sounds (2010) pp. 93–104
40. N Malyska, T Quatieri, D Sturim, in *Proc. Int. Conf. Audio Speech Signal Proc.,* vol. 1 Automatic dysphonia recognition using biologically-inspired amplitude-modulation features. (Philadelphia, USA, 2005), pp. 873–876
41. L Atlas, S Shamma, Joint acoustic and modulation frequency. EURASIP J. Appl. Signal Process. **7**, 668–675 (2003)
42. A Bondar, A Fedotchev, Concerning the amplitude modulation of the human EEG. Human Physiol. **26**(4), 393–399 (2000)
43. C Sorg, V Riedl, M Mühlau, VD Calhoun, T Eichele, L Läer, A Drzezga, H Förstl, A Kurz, C Zimmer, A Wohlschläger, Selective changes of resting-state networks in individuals at risk for Alzheimer's disease. Proc. Natl. Acad. Sci. **104**(47), 18760 (2007)
44. S Sanei, J Chambers, *EEG Signal Processing* (Wiley-Interscience, New York, 2007)
45. M Le Van Quyen, J Foucher, J Lachaux, E Rodriguez, A Lutz, J Martinerie, F Varela, Comparison of Hilbert transform and wavelet methods for the analysis of neuronal synchrony. J. Neurosci. Meth. **111**(2), 83–98 (2001)
46. Z Smith, B Delgutte, A Oxenham, Chimaeric sounds reveal dichotomies in auditory perception. Nature. **416**(6876), 87–90 (2002)
47. B Boashash, *Time Frequency Signal Analysis and Processing: A comprehensive Reference* (Elsevier, Amsterdam, 2003)
48. L Trambaiolli, A Lorena, F Fraga, R Anghinah, in *Proc ISSNIP Biosignals and Biorobotics Conf.,* vol. 1 Support Vector Machines in the Diagnosis of Alzheimer's Disease. (Vitória, Brazil, 2010), pp. 1–6
49. R Wang, K Tang, in *IEEE International Conference on Data Mining Workshops, 2009 . ICDMW'09,* vol. 1 Feature selection for maximizing the area under the ROC curve. (Florida, USA, 2009), pp. 400–405
50. C Lehmann, T Koenig, V Jelic, L Prichep, R John, L Wahlund, Y Dodge, T Dierks, Application and comparison of classification of Alzheimer's disease in electrical brain activity (EEG). J. Neurosci. Meth. **161**, 342–350 (2007)
51. W-C Lin, A case study on support vector machines versus artificial neural networks, Master's thesis, University of Pittsburgh. Pennsylvania, USA (2004)

52. V Vapnik, *The Nature of Statistical Learning Theory* (Springer-Verlag, Berlin, 1995)
53. N Cristianini, J Shawe-Taylor, *An Introduction to SVM and Other Kernel-Based Learning Methods* (Cambridge University Press, Cambridge, 2000)
54. I Witten, E Frank, *Data Mining: Practical Machine Learning Tools and Techniques* (Elsevier, Amsterdam, 2005)
55. C Babiloni, G Binetti, A Cassarino, G Dal Forno, C Del Percio, F Ferreri, R Ferri, G Frisoni, S Galderisi, K Hirata, B Lanuzza, C Miniussi, A Mucci, F Nobili, G Rodriguez, G Luca Romani, PM Rossini, Sources of cortical rhythms in adults during physiological aging: a multicentric EEG study. Human Brain Map. **27**(2), 162–172 (2006)
56. G Syed, S Eagger, J O'Brien, J Barrett, R Levy, Patterns of regional cerebral blood flow in Alzheimer's disease. Nuclear Med. Commun. **13**(9), 656–663 (1992)
57. Z Sankari, H Adeli, A Adeli, Intrahemispheric, interhemispheric, and distal EEG coherence in Alzheimer's disease. Clin. Neurophysiol (2010, in press). doi:10.1016/j.clinph.2010.09.008
58. H Adeli, S Ghosh-Dastidar, N Dadmehr, A spatio-temporal wavelet-chaos methodology for EEG-based diagnosis of Alzheimer's disease. Neurosci. Lett. **444**(2), 190–194 (2008)
59. A Ahmadlou, H Adeli, A Adeli, Fractality and a Wavelet-Chao Methodology for EEG-based Diagnosis of Alzheimer's Disease. Alzheimer Dis. Assoc. Disord. **25**(1), 85–92 (2011)
60. N Axmacher, M Henseler, O Jensen, I Weinreich, C Elger, J Fell, Cross-frequency coupling supports multi-item working memory in the human hippocampus. P. Natl. Acad. Sci. USA. **107**(7), 3228 (2010)
61. P Putman, J van Peer, I Maimari, S van der Werff, EEG theta/beta ratio in relation to fear-modulated response-inhibition, attentional control, and affective traits. Biol. Psychol. **83**(2), 73–78 (2010)
62. P Robert, G Darcourt, M Koulibaly, S Clairet, M Benoit, R Garcia, O Dechaux, J Darcourt, Lack of initiative and interest in Alzheimer's disease: a single photon emission computed tomography study. **13**(7), 729–735 (2006)
63. D Moretti, C Fracassi, M Pievani, C Geroldi, G Binetti, O Zanetti, K Sosta, P Rossini, G Frisoni, Increase of theta/gamma ratio is associated with memory impairment. Clin. Neurophysiol. **120**(2), 295–303 (2009)
64. H Payami, S Zareparsi, KR Montee, GJ Sexton, JA Kaye, TD Bird, CE Yu, EM Wijsman, LL Heston, M Litt, GD Schellenberg, Gender difference in apolipoprotein E-associated risk for familial Alzheimer disease: a possible clue to the higher incidence of Alzheimer disease in women. Am. J. Hum. Genet. **58**(4), 803 (1996)
65. C Melissant, A Ypma, E Frietman, C Stam, A method for detection of Alzheimer's disease using ICA-enhanced EEG measurements. Artif. Intell. Med. **33**(3), 209–222 (2005)

doi:10.1186/1687-6180-2012-192
Cite this article as: Falk *et al.*: **EEG amplitude modulation analysis for semi-automated diagnosis of Alzheimer's disease.** *EURASIP Journal on Advances in Signal Processing* 2012 **2012**:192.